**Liquid Crystal Displays II, SPIE v.3635, paper 18, 1999**

# The Influence of the Inter-pixel Region in Liquid Crystal Diffraction Gratings

Jay E. Stockley, Darius Subacius and Steven A. Serati

Boulder Nonlinear Systems, Inc.
450 Courtney way, #107
Lafayette, CO 80026

## ABSTRACT

An important problem associated with multiple pixel liquid crystal (LC) modulators is the incidental diffraction due to amplitude and phase gratings formed by the improperly modulated regions between electrodes. This problem becomes more of an issue as the resolution of the SLM increases and the size of the pixels begins to approach the size of the inter-pixel spacing.

We perform 2D director profile modeling in LC diffraction gratings to take into account the electrode structure and fringing electrostatic fields. The electrooptical properties of the grating are simulated and compared with experimental data. This information can be used to design addressing structures with enhanced fill factor.

The results obtained could be beneficial for applications in image processing, laser beam control, steering and adaptive optics.

**Keywords:** liquid crystal, diffractive grating, pixel structure, fringing fields, director modeling

## 1. INTRODUCTION

Liquid crystal (LC) research is primarily concentrated on display applications and most devices feature relatively large pixels compared to the inter-pixel spacing. However, the trend toward miniaturization and integration of LC displays directly onto silicon very large scale integration (VLSI) chips will result in smaller pixel size with the implication that effects in the interpixel region become more important. In addition, liquid crystals are widely used as electro-optic phase, state of polarization, and intensity modulators. Consequently, LC devices are gaining increasing importance in numerous non-display applications such as diffractive optics, optical processing, optical switching, non-mechanical beam steering, voltage controlled focusing, and adaptive optics. For many of these applications, the key technology is a Liquid crystal phase grating which exhibits the potential for high diffraction efficiency and low working voltages (<10V). The interpixel region in a liquid crystal phase grating is extremely important in terms of the electro-optic characteristics of the device. Depending on the application or implementation, interpixel effects can limit or enhance the overall performance of a liquid crystal grating.

Several researchers have experimentally and theoretically investigated the interpixel effects on the performance of LC gratings. Polarization and intensity diffraction characteristics of LC gratings have been extensively studied by He et al.[1,2]. Fringing electric fields have been employed in a diffractive device for 3-D displays[3,4] and the optical performance of an LC phase grating has also been analyzed for implementation into a schlieren projection system[5]. When the electrode spacing approaches the pixel size, the electric field distribution in the anisotropic LC medium becomes complicated and numerical techniques are required to model the electro-optic properties of the device[6,7] .

Below, we present experimental and theoretical results on the diffraction properties of a nematic LC phase grating. We discuss far field diffraction measurements and computer simulations of the LC director profile that were performed to take into account the electrode structure and fringing electric fields. Finally we describe our attempt to isolate pixels by building polymer walls between them using a technique developed by John West's group[8] .

## 2. IDEAL NLC PHASE GRATING

Here we will briefly discuss the binary rectangular phase grating where the interpixel director structure is neglected. After the ideal diffraction grating, the field distribution in the near field is given by $E_x(x) = E_{0x}(x)\exp(i \cdot \Phi(x))$, where in our case $E_{0x}(x)$ is the passive amplitude grating due to the electrode structure, and we consider it as a constant, $\Phi(x)$ is the phase transmission function. Assuming the thin grating regime the far field diffraction pattern is obtained from the Fourier transform of the transmission function. Pixel fill factor affects the spectral distribution in the Fourier domain. The far field diffraction pattern is a product of the pixel function which determines the envelope form and the array factor. For a rectangular grating with period $P$ and electrode width $L$ the envelope function is given by a so called *sinc* function:

$$f(L/P) \propto \frac{\sin(\pi \cdot m \cdot L/P)}{m \cdot L/P} \qquad (1)$$

where $m$ is the diffraction order. The ratio $L/P$ is the fill factor of the grating. In the frequency spectrum the width of the main lobe is determined by the fill factor as can be seen from (1).

An ideal rectangular binary phase grating would have maximum efficiency $\eta_{\pm 1} = 40.5\%$ in $\pm 1$ orders when the phase is $\Phi = \pi \cdot n$, $n$ is an integer. The zero order diffraction intensity is 0 and only odd diffraction maxima are present. In a blazed phase grating which is used for beam steering applications ideally 100% diffraction efficiency can be achieved .

In reality with fringing electrostatic fields in a device having a patterned electrode structure, the diffraction grating would not exhibit an ideal rectangular phase profile. Interpixel LC director orientation affects the diffraction intensities of the gratings. It is also highly undesirable in high resolution LC display applications. Not only is director profile smoothed, the ideal phase profile is disturbed by induced amplitude gratings in the interpixel region. Complex amplitude and phase modulation is obtained when director orientation is not contained in a single plane parallel to the light propagation direction, that is, when the director is characterized by both polar and azimuthal angles. As a consequence the device shows complicated polarization properties[1,2] .

The fringing fields change the pixel function, which is important for many applications such as optical processing. As the pixel width increases, the envelope function narrows and higher image frequencies are strongly attenuated[9] . For optical processing this attenuation is undesirable because the edges are high frequency details that characterize an object's shape.

For high resolution LC displays with electrode spacing of a few microns the on-pixel LC director orientation affects the neighboring off-pixels because of the fringing electrostatic fields and propagating elastic distortion.

For beam steering applications minimization of the flyback region, where the blazed phase ramp is reset back, is important to achieve the maximum efficiency[10] . This reset region is most sensitive to the fringing fields.

## 3. DIFFRACTION EXPERIMENT

A nematic transmissive LC phase grating was designed with the following parameters. One substrate is continuously coated with ITO (indium tin oxide), another one has a patterned electrode structure. The electrode width is $L = 4\mu m$ and spacing between electrodes is $P - L = 2\mu m$ . The pixels can be addressed separately to write the desired 2-D phase profile. A cell thickness of $d = 4\mu m$ is provided using glass spacers. The substrates were coated with polyimide PI-7492 from Nissan Chem. Ind. and buffed antiparallel with the buffing direction being perpendicular to the electrodes. The purpose of such a buffing direction is to keep the director deformations confined in two dimensions characterized only by the polar angle . The device was filled with nematic liquid crystal material E7 (E.Merck) with the following properties: dielectric constants $\varepsilon_p = 19.0$ , $\varepsilon_s = 5.2$, elastic constants $K_{11} = 11.1pN$ , $K_{33} = 17.1pN$ and refractive indices $n_e = 1.746$, $n_o = 1.521$. The nematic to isotropic transition temperature is at $60.5^o C$ .

To study the diffraction properties a 1-2 mm diameter He-Ne laser beam was incident normally on the LC grating. Incident light polarization is set by a rotating polarizer. The analyzer is set behind the device to

check the intensities of different polarizations of diffracted light. Light intensity is measured using a ThorLabs photodetector placed at the positions of the diffraction maxima.

Applied voltage causes the reorientation of the LC molecules. The orientation profile depends on the voltage. So, the phase profile $\Phi(x)$ is electrically varied and the diffraction intensities are changed. For the binary grating every second pixel is addressed and the voltage on the pixels between is set to the ground (or cover glass) voltage (usually $0V$ ). To write a blazed phase profile different voltage values are applied on each electrode, up to the number of electrodes per period.

Figure 1a shows the diffracted light intensity dependence for the $0^{th}$, $+1^{st}$ and $+2^{nd}$ orders on the applied voltage for binary addressing. The incident light is linearly polarized parallel to the electrode structure. All light intensities in this and following figures are normalized by the zero order light intensity when no voltage is applied to the device. Figure 1b illustrates the diffraction dependence on voltage for the incident light polarized perpendicular to the electrodes. Ideally a phase grating is formed only for light polarized parallel to the electrodes when the director deformations are contained in the xz plane and can be described by the polar angle only. Fig.1b shows that at higher voltages $U > 5V$ more complicated director orientation is obtained with the director going out of the xz plane. In Fig.1a the $1^{st}$ order diffraction reaches maximum intensity at approximately 3.4V, which corresponds to the phase modulation depth of $\pi$ . At the same time the intensity for the $0^{th}$ order is not zero as it should be for an ideal phase grating and reaches a minimum at slightly different voltage. The intensity of the $2^{nd}$ order is not zero what shows that the phase profile is not rectangular and also a double periodicity modulation may be present. The diffracted light up to $U > 5V$ is linearly polarized with the same polarization direction as the incident light. At higher voltages the diffracted light is generally elliptically polarized, so that polarization coupling occurs as discussed by He et al. [1,2] .

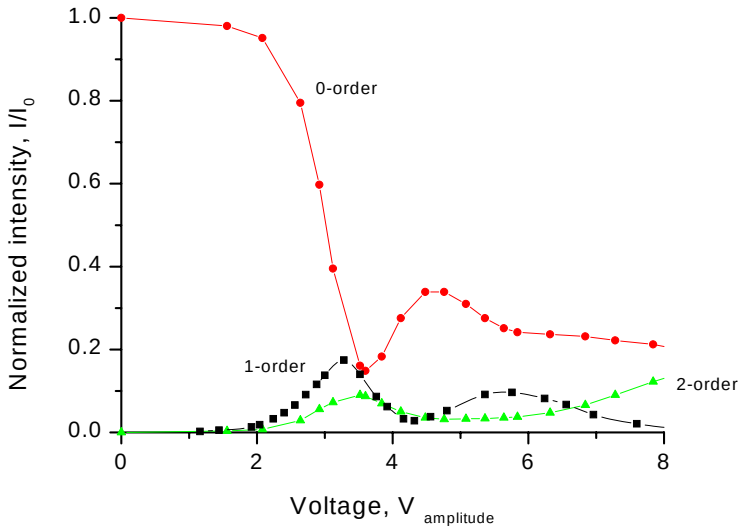


Fig.1a. Experimental diffraction intensity dependence on applied voltage for 0, +1 and +2 orders for the light polarized parallel to the electrodes. The intensities are normalized to the zero order intensity in the absence of the field.

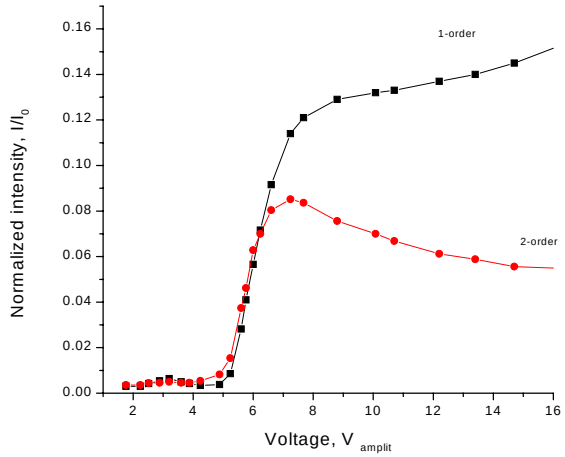


Fig. 1b. Experimental diffraction intensity dependence on applied voltage for 0, +1 and +2 orders for the light polarized perpendicular to the electrodes.

In figure 2 the diffraction intensities for different orders are presented at the applied voltage which correspond to the maximum intensity of the 1st order. The most striking feature is a non symmetric diffraction pattern, which probably can be explained by the director pretilt angle, so that LC director deformations for one direction are more favorable energetically. Incident light is linearly polarized parallel to the electrodes. Diffraction intensities of the ±1 orders do not reach their theoretical value of 40.5%.

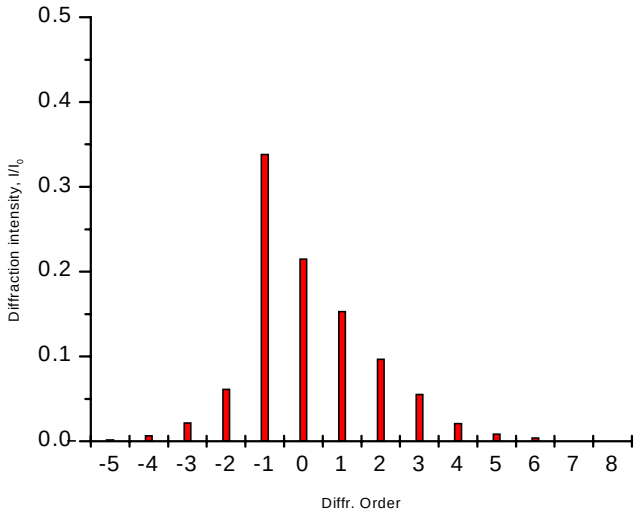


Fig.2. Diffraction intensities for different orders. Applied voltage corresponds to the max intensity of the 1st order.

## 4. DIRECTOR PROFILE MODELING

We used numerical simulations to take into account the fringing fields and LC director distortions in the inter-pixel region for 2-D model considering only the case when director deformations are confined in the xz plane. We have used a self-consistent model for the effects of an inhomogeneous electric field on the nematic liquid crystal grating. The model and simulation results are presented below.

For high resolution LC modulators the simplifying approximation that the medium is a homogeneous dielectric is not valid anymore. To obtain information about the extent of fringing fields, a quantitative analysis needs to consider the anisotropy of the liquid crystal. It is necessary to understand the quantitative behavior of the device in order to obtain an accurate representation of the phase profile.

The self-consistent model described here uses a finite difference approach[6,7] . The medium is divided into a grid of points. For an anisotropic medium, the field is reduced due to dipole interactions. Laplace's equation becomes

$$div\left(\tilde{\varepsilon}\ grad\ \Phi\right) = 0 \tag{2}$$

where $\Phi$ is the electrostatic potential and $\tilde{\varepsilon}$ is the dielectric tensor.

First, an initial director distribution is assumed, which determines the dielectric tensor that is used in Laplace's equation. Taylor series expansion of Equation (2) about the grid points results in a finite difference equation which can be used to arrive at an iterative solution for the electrostatic potential.

$$\Phi(i,j) = \frac{1}{2(\varepsilon_p+\varepsilon_s)}\left[\varepsilon_p\Phi(i,j+d)+\varepsilon_s\Phi(i+d,j)+\varepsilon_p\Phi(i,j-d)+\varepsilon_s\Phi(i-d,j)\right] \tag{3}$$

Here, the indices i and j are the grid indices in the z and x (propagation direction and transverse direction) respectively. The subscripts p and s stand for parallel and perpendicular, respectively, and $d$ is the distance between grid points (here assumed to be the same in both the x and z directions).

The electromagnetic field lines are determined from the gradient of the electrostatic potential.

$$\vec{E} = -\nabla\Phi \tag{4}$$

Once the field is known, the director distribution for the nematic liquid crystals is determined using a system of relaxation equations of elliptic form:

$$\gamma\frac{\partial}{\partial t}\left[n_a n_b\right] = K\,\nabla^2\left[n_a n_b\right] + \frac{\Delta\varepsilon}{4\pi}E_a E_b \tag{5}$$

Here $n_a$ and $n_b$ are the director components in the x or z direction. The subscripts a and b can both be x, z, or one of each. The viscosity coefficient is $\gamma$ and K is the Frank-Oseen elastic constant. The electric field components are $E_a$ and $E_b$. Finally, $\Delta\varepsilon$ is the dielectric anisotropy. The equations are subject to the constraint that $n_x n_x + n_z n_z = 1$. The director distribution (obtained from the system of equations typified by Equation 5 above) is used to calculate a revised dielectric permittivity that is used in a new iteration of Laplace's equation. The finite difference expansion of the generalized Laplace's equation for an inhomogeneous anisotropic medium becomes

$$\Phi(i,j) = \frac{1}{\left(2\varepsilon_s+\Delta\varepsilon\left[n_x n_x+n_z n_z\right]\right)}\left\{\begin{array}{l}
\Phi(i,j+d)\left[\dfrac{\varepsilon_s+\Delta\varepsilon\, n_x n_x}{2}+\dfrac{\Delta\varepsilon}{4}\left(\dfrac{\partial n_x n_x}{\partial x}+\dfrac{\partial n_x n_z}{\partial z}\right)\right] \\
+\Phi(i+d,j)\left[\dfrac{\varepsilon_s+\Delta\varepsilon\, n_z n_z}{2}+\dfrac{\Delta\varepsilon}{4}\left(\dfrac{\partial n_x n_z}{\partial x}+\dfrac{\partial n_z n_z}{\partial z}\right)\right] \\
+\Phi(i,j-d)\left[\dfrac{\varepsilon_s+\Delta\varepsilon\, n_x n_x}{2}-\dfrac{\Delta\varepsilon}{4}\left(\dfrac{\partial n_x n_x}{\partial x}+\dfrac{\partial n_x n_z}{\partial z}\right)\right] \\
+\Phi(i-d,j)\left[\dfrac{\varepsilon_s+\Delta\varepsilon\, n_z n_z}{2}-\dfrac{\Delta\varepsilon}{4}\left(\dfrac{\partial n_x n_z}{\partial x}+\dfrac{\partial n_z n_z}{\partial z}\right)\right] \\
+\dfrac{\Delta\varepsilon\, n_x n_z}{4}\left[\begin{array}{l}\Phi(i+d,j+d)-\Phi(i+d,j-d)\\+\Phi(i-d,j-d)-\Phi(i-d,j+d)\end{array}\right]
\end{array}\right\} . \tag{6}$$

The basic algorithm is to begin with the dielectric tensor due to the director distribution at time t=0. Then, the initial estimate of the electrostatic potential is determined via convergence of the finite element formalism using Equation 3. The electric field is determined from the gradient of the electrostatic potential (Equation 4) and a director distribution is computed using the forward time, central difference method applied to the system of equations typified in Equation 5. The new director distribution is used to solve the inhomogeneous finite difference representation of Laplace's Equation given in Equation 6. From the electrostatic potential determined by convergence of Equation 6, the electrostatic field is recalculated using Equation 4 and substituted back into the system of equations used to determine the director distribution. This process is repeated until the potential function and the director distribution simultaneously converge.

In Figure 3 the LC director profile obtained by simulation for applied voltage $U = 0.5V$ is presented. In this figure and following modeling figures the electrode array corresponds to our experimental device and consists of 4 μm lines and 2 μm spaces. The thickness of the liquid crystal medium is taken as 4 μm. Two electrodes are shown in the 12 μm region investigated here. The first electrode is from 0.75μm to 4.75 μm and the voltage is set to 0V. The second electrode is from 6.75μm to 10.75 μm and the voltage is set to some value. The top electrode is the ground electrode and voltage is always set to 0V. Boundaries to the left and right are assumed to wrap around (i.e. the pattern repeats itself in either direction). Initial LC alignment is planar along the x-axis with a small pretilt angle, the deformations are contained in the xz plane. Everywhere in simulations infinite anchoring energy is assumed. Solid lines represent the equipotential lines.

In Figure 4a the director profile at $U = 5V$ in binary addressing is presented. Figure 4b illustrates the phase transmission function of the binary LC grating shown in Fig.4a. To obtain the phase profile $\Phi(x)$ in the near field we used a Jones matrix technique. The far field diffraction pattern can be obtained by the Fourier transform. Figures 3 and 4 show that the LC director in the electrode region is switched, but at the same time the deformations propagate into the interpixel region, where the director field is also slightly deformed from the initial orientation. The phase profile (Fig.4b.) is not a rectangular grating, but a smoothed almost sinusoidal wave. From our modeling we could not obtain the strongly non symmetric diffraction pattern as observed experimentally, Fig.2. One possible explanation could be the disclinations in the director field.

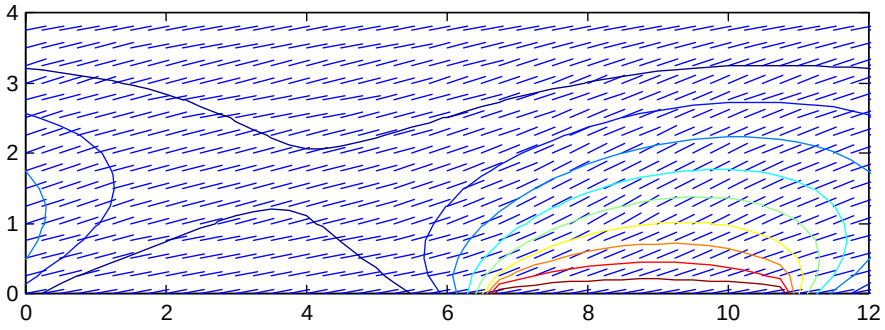


Fig. 3. Director profile and electrostatic potential lines for a 0.5V applied to the electrode array in binary addressing.

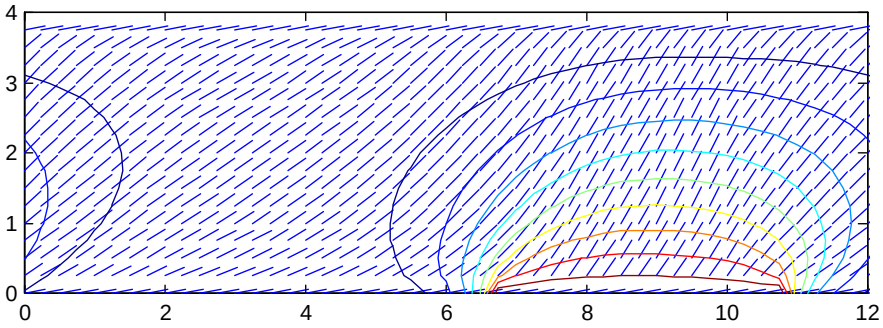


Fig. 4a. Director profile and electrostatic potential lines for a 5V applied to the electrode array in binary addressing.

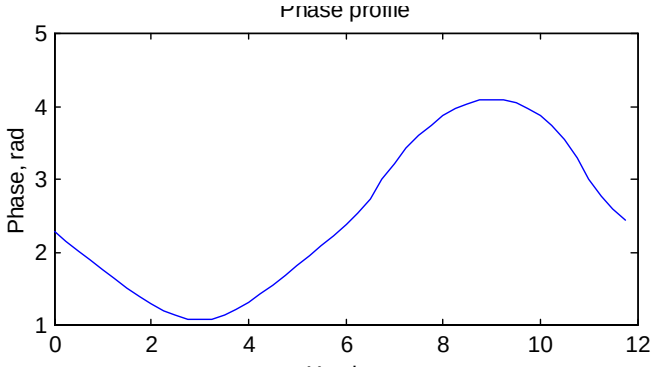


Fig.4b. Phase transmission function of the binary grating presented in Fig. 4a.

## 5. PIXEL SEPARATION

In this section we describe results of our attempt to isolate the pixels and director modeling results with separation walls.

To build the polymer walls we used an approach developed by J.West's group at the Liquid Crystal Institute [8].

Mixtures were composed of UV curable monomer (isotropic material such as Norland Optical Adhesive NOA65) and nematic liquid crystal E7 in a ratio 2:1. We used the identical procedure as described in reference [8].

Application of a patterned electric field during phase separation and subsequent blanket UV- irradiation result in formation of polymer walls in the interpixel regions of the SLM. In these mixtures phase separation usually occurs upon cooling from the isotropic state into a heterogeneous state. The phase separation reduces the concentration of LC in the interpixel region. One possible physical mechanism of LC and monomer separation is different dielectric constants of the materials [8]. In the electrode region the electrostatic energy density stored by the single pixel capacitor could be approximately given by $W = \frac{1}{2}\int_V \varepsilon E^2 dv$, where $\varepsilon$ is the dielectric constant of the material, $E$ is the electric field strength, $V$ is pixel volume. The energy is minimized by forcing the material with higher $\varepsilon$ out of the pixel region. As a consequence electric field strength and dielectric properties of LC and monomer determine the grating formation.

Figures 5a and 5b show the obtained LC/polymer grating with LC separated in the electrode region and polymer in the interpixel region. Polymer walls are optically isotropic and do not transmit light between crossed polarizers. LC regions are birefringent and become bright when the device is rotated between crossed polarizers, Fig 5b. In Figure 5a the bright areas near polymer walls correspond to the complicated 3-D director orientation in that region. These distortions could be explained by the anchoring of LC molecules on polymer walls. In such a polymer/LC structure LC regions are confined not only by the cell substrates but also by the polymer walls in the interpixel region. In Figure5b the area with the unaddressed electrode is presented where the LC droplets are dispersed isotropically in polymer matrix as in the polymer dispersed LC devices.

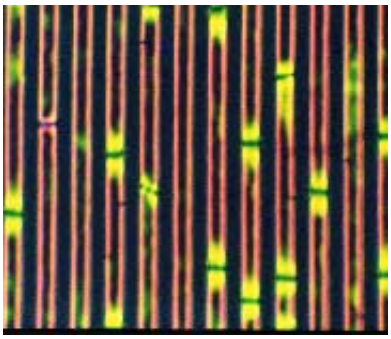

Fig.5a.

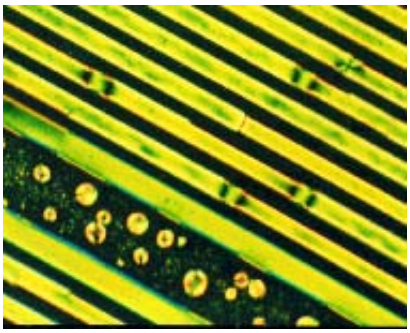

Fig.5b.

Fig.5 Microscopic photographs of the liquid crystal regions separated by the isotropic polymer walls between crossed polarizers. Fig.5a. walls are parallel to the analyzer , Fig.5b. walls are rotated for some angle from analyzer direction. Width of the electrodes is 12μm and spacing between is 12μm, cell thickness is 4μm.

Polymer wall formation was attempted for higher resolution devices. However we encountered a problem with the fringing electrostatic fields. As shown in Fig.3 and 4a the field potential lines penetrate into the interpixel region. To build isolating polymer walls we need the E-field to be localized in the pixel region, so that for higher resolution devices this technique can be used only for certain cell thickness depending on the electrode period. There are other possible ways to isolate pixels, like photolithographic etching, etc. To illustrate the results of the pixel separation, we performed LC director simulations including idealized walls between electrodes, taking into account the anchoring on the polymer surface.

In Figure 6a the LC director profile in the cell with idealized walls is presented at $U = 0V$ . The walls are strictly in the interpixel region. The LC anchoring on the walls is planar with the director aligned along the z-axis (perpendicular to the cell substrate). LC anchoring on the substrates is planar with a small pretilt angle. The deformations are contained in the xz plane. Infinite anchoring energy is assumed on all boundaries. As can be seen from this figure the wall anchoring significantly affects the initial director orientation in the absence of the field. Director orientation is distorted from the initial planar orientation to satisfy boundary conditions. Figure 6b represents the near field phase profile of the LC director obtained from Fig.6a. For the interpixel walls we assumed the refractive index $n = n_e$ of LC. Also we assumed the wall to be optically isotropic.

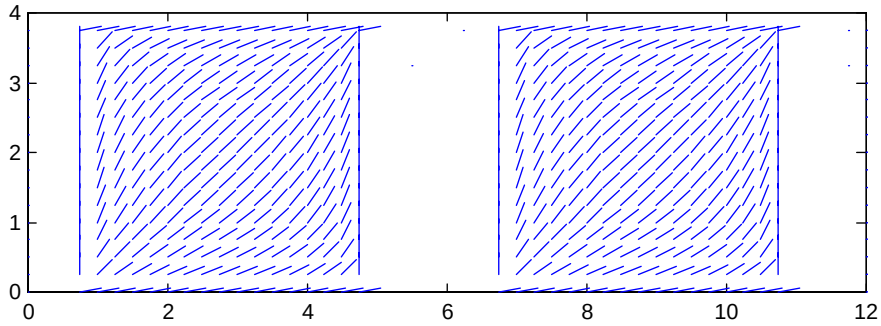


Fig. 6a LC director profile in the array with pixel separated structure in the absence of the field. Empty areas represent the isotropic walls.

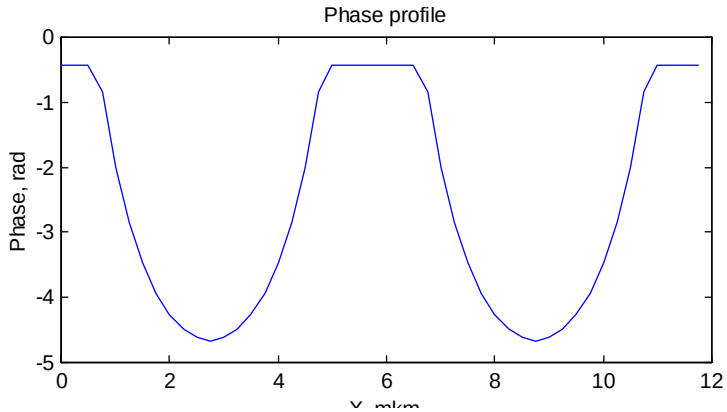


Fig. 6b Phase transmission profile in the near field corresponding to the director profile of Fig.6a.

Figure 7a illustrates the director orientation in the array with separated pixels at the applied voltage of $U = 5V$ . On the left pixel a voltage $U = 0V$ is applied . Although the fringing electrostatic field from the right pixel penetrates into this region, it is insufficient to switch the LC director . The right pixel is switched on, with the director aligned along the field. In Figure 7b the corresponding near field phase profile is presented.

This proves that LC orientation in one pixel does not affect the orientation in the neighboring pixel. This pixel isolation may have applications in diffractive and adaptive optics where sharp phase profiles can be desirable.

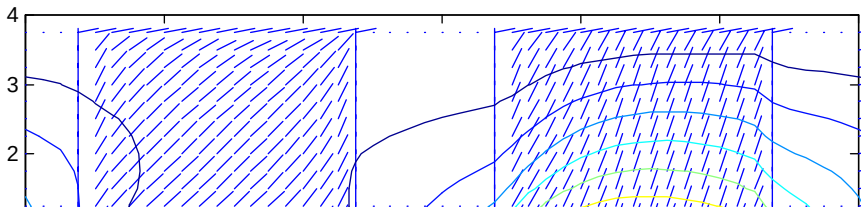

Fig. 7a LC director profile in the array with pixel separated structure in binary addressing, applied voltage $U = 5V$ . Empty areas represent the isotropic walls.

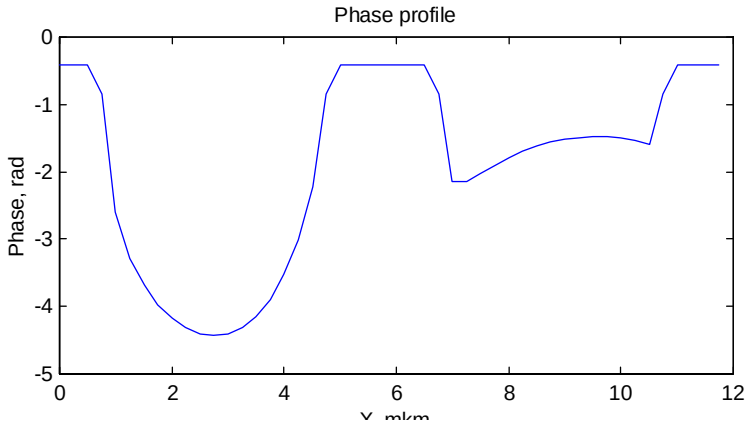


Fig. 7b Phase transmission profile in the near field corresponding to the director profile of Fig.7a.

## 6. CONCLUSIONS

We have discussed the influence of the inter-pixel region in a liquid crystal phase grating. The diffractive properties of this device were experimentally investigated. Measurements of the far field diffraction pattern produced by addressing the grating demonstrate that polarization coupling occurs. This phenomenon can be attributed to improperly modulated regions between electrodes. To more clearly understand the interplay of the electrode structure and fringing electrostatic fields, we have performed liquid crystal director modeling. Model results show that director deformations elastically propagate into the interpixel region causing undesired phase and amplitude distortions of the propagating light. Our simulations also indicate that the pixels can be electrically and elastically isolated by designing walls between them. Moreover, anchoring forces associated with these walls can effect the quiescent director distribution. Using the technique of structured electric-field phase separation of an LC/polymer system, polymer walls in the inter-pixel region of an ITO electrode array were built. Our successful attempts at polymer wall formation have so far been limited to relatively low resolution gratings. As the theoretical study and physical implementation of liquid crystal gratings continues, interesting effects such as the pixel isolation discussed here could result in applications beneficial to high resolution displays, dynamic diffractive elements, beam steering and adaptive optics.

## 7. ACKNOWLEDGMENTS

This work is supported by Wright Laboratory, Wright-Patterson AFB contract number F33615-97-C-1140. Part of this research was also funded by Phillips Laboratory, Kirtland AFB, contract #F29601-98-C-0045.

## 8. REFERENCES

1. Z. He, T. Nose, S. Sato, "Polarization properties of an amplitude nematic liquid crystal grating", *Opt. Eng.* **37**, pp.2885-2898, 1998.

2. Z. He, T. Nose, S. Sato, "Diffraction and polarization properties of a liquid crystal grating", *Jpn. J. Appl. Phys.* **34**, pp.2392-2395, 1996.

3. J.H. Kulick, J.M. Jarem, R.G. Lindquist, S.T. Kowel, M.W. Friends, T.M. Leslie, "Electrostatic and diffraction analysis of a liquid-crystal device utilizing fringing fields: applications to three-dimensional displays", *Appl. Opt.* **34**, pp. 1901-1921, 1995.

4. R.G. Lindquist, J.H. Kulick, G.P. Nordin, J.M. Jarem, S.T. Kowel, M.W. Friends, "High-resolution liquid-crystal phase grating formed by fringing fields from interdigitated electrodes", *Opt. Lett.* **19**, pp. 670-672, 1994.

5. M.W. Fritsch, C. Kohler, G. Haas, H. Wohler, D.A. Mlynski, "Diffraction properties of rectangular phase gratings in a liquid crystal phase modulator", *Mol. Cryst. Liq. Cryst.* **198**, pp. 1-14, 1991.

6. A. Kilian and S. Hess, "Derivation and application of an algorithm for the numerical calculation of the local orientation of nematic liquid crystals", *Z. Naturforsch.* **44a**, pp. 693-703, 1989.

7. G. Haas, H. Wohler, M. W. Fritsch and D.A. Mlynski, "Simulation of two-dimensional nematic director structures in inhomogeneous electric fields", *Mol. Cryst. Liq. Cryst.* **198**, pp. 15-28, 1991.

8. Y. Kim, J.Francl, B. Taheri and J.L. West, "A method for the formation of polymer walls in liquid crystal/polymer mixtures", *Appl. Phys. Lett.* **72**, pp. 2253-2255, 1998.

9. S. Serati and K. Bauchert, "Analog spatial light modulators advances and applications", *SPIE* **3292**, pp.1-11, 1998.

10. P.F. Mcmanamon, T.A. Dorschner, D.L. Corkum, L.J. Friedman, D.S. Hobbs, M. Holz, S. Liberman, N.Q. Nguyen, D.P. Resler, R.C. Sharp, E.A. Watson, "Optical phased array technology", *Proc. IEEE* **84**, pp. 268-298, 1996.